Efficient Large-Domain MoM Solutions to Electrically Large Practical EM Problems

Branislav M. Notaroš, *Member, IEEE*, Branko D. Popović, *Member, IEEE*, Jan Peeters Weem, *Student Member, IEEE*, Robert A. Brown, and Zoya Popović, *Senior Member, IEEE*

Abstract—A numerical method is presented for the analysis and design of a wide variety of electromagnetic (EM) structures consisting of dielectric and conducting parts of arbitrary shapes. The method is based on the integral-equation formulation in frequency domain, and represents a large-domain (high-order expansion) Galerkin-type version of the method of moments (MoM). The method is formulated in two versions concerning the type of the equivalence (volume and surface) utilized in the treatment of the dielectric parts of the structure. The generality, versatility, accuracy, and practicality of the method and code are demonstrated on four very diverse, electrically large, and complex EM problems. The examples are: an X-band reflector antenna modeled after a bat's ear, which is about $11\lambda^3$ large at X-band, a broad-band (0.5–4.5 GHz) nested array of crossed loaded dipoles, an EM system consisting of a dipole antenna and a human body, and a broad-band (1–5 GHz) microstrip-fed Vivaldi antenna with a high-permittivity dielectric substrate. The central processing unit times with a modest personal computer are on the order of several minutes for a single-frequency application.

Index Terms—Antennas, CAD, method of moments, numerical analysis.

I. INTRODUCTION

MOST OF THE existing frequency-domain integral-equation methods for analysis of arbitrary three-dimensional (3-D) electromagnetic (EM) structures are subdomain (small-domain)-type methods of moments. More precisely, the structure is approximated by many electrically small geometrical elements (on the order of $\lambda/10$ in each dimension), with low-order expansion functions for currents [1]–[7]. In the authors' opinion, an entire-domain approach can greatly extend the versatility, accuracy, reliability, and efficiency of moment methods. More precisely, the entire-domain (large-domain) technique utilizes high-order expansion functions defined in electrically large geometrical elements (a few wavelengths in each dimension) [8]–[15].

This paper outlines a large-domain method of moments (MoM) for analysis of structures composed of arbitrarily excited and loaded dielectric and conducting bodies of arbitrary shapes.

It is based on a frequency-domain integral-equation formulation. Metallic parts of the structure are treated by introducing surface electric conduction currents over conducting surfaces as unknown quantities in the system of coupled integral equations. The method has two versions concerning the type of the equivalence invoked in the treatment of the dielectric parts of the structure. The first version utilizes the volume equivalence principle to compensate the dielectric materials by the actual induced volume electric currents in a vacuum. These currents represent the unknown quantities to be determined in the solution procedure [9]–[13]. The other version of the method, which is presented for the first time in this paper, invokes the surface equivalence principle (generalized Huygens' principle), and utilizes as unknown quantities equivalent (artificial) electric and magnetic surface currents over boundary surfaces between the homogeneous regions of the structure. Note that for purely metallic structures in a vacuum, the two versions of the method are identical. In both versions, the geometry is modeled by flexible parametric elements with high-order polynomial expansions for the approximation of currents, enabling electrically large elements to be used. In this manner the resulting number of unknowns for a given problem is reduced by an order of magnitude when compared to small-domain calculation.

This paper is aimed at demonstrating that the MoM, if well designed and carefully optimized, can be a highly efficient and reliable tool for the analysis and design of a wide class of complex 3-D EM structures. The MoM is often thought to be the method for solving "canonical" problems of subwavelength size. The large-domain (high-order current approximation) approach, used surprisingly rarely, promotes the applicability of the MoM to real-world problems. As examples, this paper presents: 1) the analysis of an antenna modeled after a bat's ear, about $11\lambda^3$ in size at 10 GHz; 2) the design of a broad-band nested loaded dipole array (operating from 0.5 to 4.5 GHz); 3) the analysis of an EM system consisting of a dipole antenna and a human body; and 4) the analysis of a broad-band microstrip-fed Vivaldi slot with high-permittivity dielectric substrate operating from 1 to 5 GHz. All the simulations are performed on a modest PC (Pentium 166 MHz with 16-MB RAM memory), with CPU times on the order of several minutes for a single-frequency application.

II. INTEGRAL EQUATIONS FOR CURRENTS

We first describe the theoretical basis of our approach. Consider a structure consisting of arbitrarily shaped metallic and dielectric parts. Let the structure be situated in a time–harmonic

incident (impressed) field of complex electric field intensity E_i and angular frequency ω. The integral-equation numerical analysis of such a structure can be performed by employing either the volume or the surface equivalence principle. The volume equivalence principle is described first, as it is conceptually much simpler.

A. Volume Equivalence Principle

The incident field induces conduction and polarization currents, of density J, in the structure volume. According to the volume equivalence principle, these currents can be considered to be in a vacuum so that the scattered electric field E can be expressed in terms of these currents through integrals that involve the free-space Green's function [9]. For the perfectly conducting parts of the structure, the volume currents can be replaced by surface currents of density J_s over the perfect electrical conductor (PEC) surfaces.

Generalized local Ohm's law and boundary condition on the PEC give the following relations:

$$\frac{J}{\sigma_e} - E(J, J_s) = E_i \quad \text{(inside dielectrics)} \tag{1}$$

$$-\big[E(J, J_s)\big]_{\text{tang}} = (E_i)_{\text{tang}} \quad \text{(over PEC surfaces)} \tag{2}$$

where $\sigma_e = \sigma + j\omega(\epsilon - \epsilon_0)$ is the dielectric equivalent complex conductivity. Note that the dielectrics can be both inhomogeneous and lossy. The integral equations (1) and (2), which include the integral expressions for the scattered field $E(J, J_s)$, represent a system of coupled simultaneous electric-field integral equations with J and J_s as unknowns.

B. Surface Equivalence Principle

Suppose now that the system under consideration consists of N homogeneous dielectric regions (domains), which generally include PEC surfaces. One of the domains is the external space (most often air, but can also be water, real ground, etc.) surrounding the structure. We can use the surface equivalence principle (generalized Huygens' principle) to break the system into N subsystems, each of them representing one of the dielectric regions, together with the belonging PEC surfaces, with the remaining space being filled with the same medium. To achieve this, a layer of equivalent (artificial) surface electric currents of density J_s and a layer of equivalent (artificial) surface magnetic currents of density M_s must be placed on the boundary surface of each dielectric region, with the objective to produce a zero total field in the surrounding space. These current densities are given by

$$J_s = n \times H_{\text{tot}}$$
$$M_s = -n \times E_{\text{tot}} \tag{3}$$

where n is the inward normal on the dielectric surface and E_{tot} and H_{tot} are the total electric and magnetic fields at the surface. On the PEC surfaces, only the (actual) surface electric currents (J_s) exist. The scattered electric and magnetic fields in the region of complex permittivity ϵ and complex permeability μ can be expressed in terms of these currents as follows:

$$E = E(J_s, M_s, \epsilon, \mu) = -j\omega A - \nabla\Phi - \frac{1}{\epsilon}\nabla \times F \tag{4}$$

$$H = H(J_s, M_s, \epsilon, \mu) = -j\omega F - \nabla U + \frac{1}{\mu}\nabla \times A \tag{5}$$

$$A = \mu \int_S J_s g\, dS$$

$$F = \epsilon \int_S M_s g\, dS$$

$$\Phi = \frac{j}{\omega\epsilon}\int_S \nabla_s \cdot J_s g\, dS$$

$$U = \frac{j}{\omega\mu}\int_S \nabla_s \cdot M_s g\, dS. \tag{6}$$

Here, A and F are the magnetic and electric vector potential, while Φ and U are the electric and magnetic scalar potential, respectively. S is the boundary surface of the region considered, and g is the Green's function for the unbounded homogeneous medium of parameters ϵ and μ as follows:

$$g = \frac{e^{-\gamma R}}{4\pi R} \quad \gamma = j\omega\sqrt{\epsilon\mu} \tag{7}$$

γ being the propagation coefficient in the medium and R the distance of the field point from the source point.

The boundary conditions for the tangential components of the total electric and magnetic field vectors on the boundary surface between dielectric domains 1 and 2 yield

$$\big[E(J_s, M_s, \epsilon_1, \mu_1)\big]_{\text{tang}} + (E_i)_{\text{tang}}$$
$$= \big[E(-J_s, -M_s, \epsilon_2, \mu_2)\big]_{\text{tang}} \quad \text{(on surface 1–2)} \tag{8}$$

$$\big[H(J_s, M_s, \epsilon_1, \mu_1)\big]_{\text{tang}} + (H_i)_{\text{tang}}$$
$$= \big[H(-J_s, -M_s, \epsilon_2, \mu_2)\big]_{\text{tang}} \quad \text{(on surface 1–2)} \tag{9}$$

where we assume that the incident/impressed field is present only in domain 1. The negative sign on the equivalent currents in the expressions of the fields in domain 2 is due to the opposite directions of the normal n in (3) when applying the equivalence principle for the two adjacent domains. On the PEC surfaces, we reduce boundary conditions (8) and (9) to $(E_{\text{tot}})_{\text{tang}} = 0$ [as in (2)] only. Having in mind the integral expressions for the fields in (4)–(7), (8) and (9) represent a set of coupled electric-/magnetic-field integral equations for J_s and M_s as unknowns.

Note that for purely metallic structures in air, principles A and B lead to the same integral equation. Consequently, the corresponding two versions of our numerical method are identical in such cases.

III. GEOMETRICAL MODELING

We approximate all the surfaces (PEC and dielectric surfaces) by a system of bilinear quadrilaterals. A bilinear quadrilateral (Fig. 1) is defined uniquely by its four vertices, which can be positioned arbitrarily in space. The parametric equation of the quadrilateral in a local (generally nonorthogonal) u–v coordinate system in the figure is

$$r(u, v) = \big[r_1(1-u)(1-v) + r_2(u+1)(1-v)$$
$$+ r_3(1-u)(v+1) + r_4(u+1)(v+1)\big]/4$$
$$= r_c + r_u u + r_v v + r_{uv} uv, \quad -1 \le u, v \le 1 \tag{10}$$

Fig. 1.   Bilinear quadrilateral.

Fig. 2.   Trilinear hexahedron.

Fig. 3.   Four characteristic terms of polynomial expansion in (11) defined on two adjacent bilinear sufraces. Function $F1$ is defined on surface 1 with $i = 1$ and $j = 2$, $F2$ is defined on surface 2 with $i = 0$ and $j = 2$, $F3$ is defined on surface 1 with $i = 2$ and $j = 2$, $F4$ is defined on surface 2 with $i = 3$ and $j = 3$. $F1$ and $F2$ are the same along the common edge, and the corresponding polynomial coefficients are common for the two surfaces. $F3$ and $F4$ are zero along the common edge.
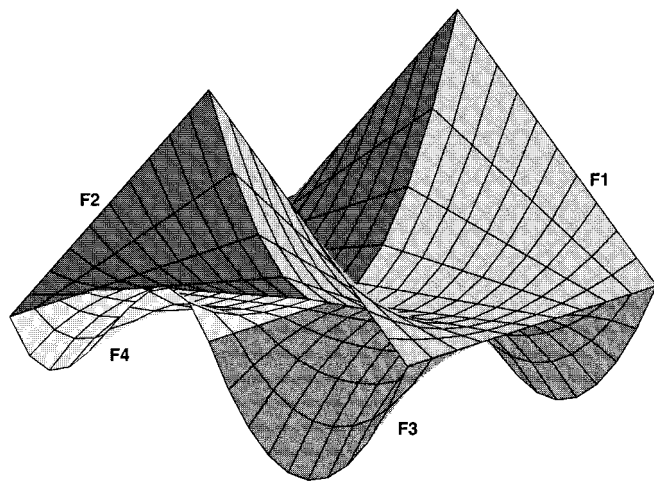
where $\boldsymbol{r}(u, v)$ is the position vector of a quadrilateral point, and $\boldsymbol{r}_c, \boldsymbol{r}_u, \boldsymbol{r}_v$, and $\boldsymbol{r}_{uv}$ are constant vectors that can be expressed in terms of the position vectors of the quadrilateral vertices $\boldsymbol{r}_1, \boldsymbol{r}_2, \boldsymbol{r}_3$, and $\boldsymbol{r}_4$. The quadrilateral edges and all parametric coordinate lines are straight, but, in general, its surface is curved (inflexed).

As the basic volume element for the approximation of (inhomogeneous) dielectric bodies, we adopt a trilinear hexahedron, sketched in Fig. 2 [9]. This is a body determined solely by eight arbitrary points in space, which represent its vertices. The hexahedron edges and all coordinate lines are straight, while its sides (bilinear quadrilaterals) in the general case are curved.

IV. HIGH-ORDER EXPANSION FUNCTIONS FOR CURRENTS

We approximate the u-componenet of vector $\boldsymbol{J}_s$ over bilinear surfaces by the following two-dimensional (2-D) large-domain (high-order) polynomial expansion in the coordinates u and v:

$$\boldsymbol{J}_{su}(u, v) = \frac{\boldsymbol{e}_u}{|\boldsymbol{e}_u \times \boldsymbol{e}_v|} \sum_{i=0}^{N_u} \sum_{j=0}^{N_v-1}$$
$$\cdot a_{uij} \begin{cases} 1-u, & i=0 \\ u+1, & i=1 \\ u^i-1, & i=2, 4, \ldots, N_u(2) \\ u^i-u, & i=3, 5, \ldots, N_u(2) \end{cases} v^j,$$
$$\boldsymbol{e}_u = \frac{d\boldsymbol{r}}{du}; \quad \boldsymbol{e}_v = \frac{d\boldsymbol{r}}{dv}; \quad -1 \leq u, v \leq 1 \tag{11}$$

where $\boldsymbol{r}$ is defined in (10), N_u and N_v are the adopted degrees of the polynomial, and a_{uij} are unknown complex coefficients to be determined. Similar expressions are used for the v-component of $\boldsymbol{J}_s$, as well as for both components of $\boldsymbol{M}_s$. The expansions satisfy automatically the current-continuity condition for $\boldsymbol{J}_s$ and/or $\boldsymbol{M}_s$ along an edge shared by (metallic and dielectric) bilinear surfaces. This improves the solution greatly. More precisely, the vector basis functions, which include terms $(1\pm u)v^j$ and $u^i(1\pm v)$ serve for the automatic adjustment of the condition at the quadrilateral interconnections (and free edges). Note that the angle between the u and v coordinate lines at the interconnection generally varies from one bilinear quadrilateral to another. All other basis functions are zero at the quadrilateral edges, and serve for improving the current approximation over the surface. Shown in Fig. 3 are four characteristic polynomial functions defined on two adjacent bilinear surfaces.

The u-, v-, and w-components of $\boldsymbol{J}$ inside trilinear hexahedrons (in the volume-equivalence approach) are approximated by large-domain basis functions, which represent a 3-D generalization of polynomials in (11) [9]. Note that another possibility within the volume-equivalence approach would be to utilize thin-wall volume modeling of dielectric bodies with 2-D polynomial basis functions in analogy to using rooftop functions defined on the wall cells, as proposed in [4] and [5].

Finally, if the EM structure contains wire-like PEC surfaces, we model them by straight wire segments, and utilize the corresponding one-dimensional (1-D) polynomials for the approximation of the line–current intensity $I(u)$ along the segments [11].

The polynomial degrees N_u, N_v, and N_w can be high, depending on the electrical size of the element in the u, v, and w directions, respectively. Of course, the elements cannot be arbitrarily large. Our strategy is to approximate the structure geometry by geometrical elements (wire segments, bilinear quadrilaterals, and trilinear hexahedrons) that are as large as

possible, and then to subdivide any electrically very large elements into smaller ones in order to achieve minimal total number of unknowns for the desired accuracy. It is impossible to find a unique criterion for the element size for an optimal solution for all cases. After extensive numerical experiments, however, we adopted 2λ to be the general limit in the code beyond which the element is subdivided in that particular dimension. The maximal polynomial degree is adopted to be eight. Within a multiple-frequency simulation, the discretization is automatically repeated for every new frequency.

By adopting $N_u = N_v = 1$ in (11) (the first two terms only) for all bilinear surfaces in the model, we obtain a small-domain version of our method, with rooftop basis functions [6] defined on bilinear quadrilaterals that cannot extend more than $\lambda/10$ in each direction. Similarly, with $N_u = N_v = N_w = 1$, our polynomial volume basis functions degenerate into 3-D rooftop functions [2] defined in electrically small trilinear hexahedrons.

V. OPTIMIZATION OF FIELD COMPUTATIONS

Although the large-domain MoM is far superior to the small-domain MoM when comparing the number of unknowns, the large-domain MoM expressions for the fields entering the integral equations and the resulting system matrix elements tend to be quite complicated and their calculation extremely time consuming if evaluated directly. We performed, therefore, an extensive analytical manipulations of these expressions [13] and careful optimization of the computer code, in order to achieve a substantial reduction of the CPU time per unknown.

The unknown current-distribution coefficients in the expansions for I, $\boldsymbol{J}_s$, $\boldsymbol{M}_s$, and $\boldsymbol{J}$ are obtained by solving the system of coupled integral equations by means of the Galerkin testing procedure [16]. The Galerkin generalized impedances (the system matrix elements) can be represented as linear combinations of 18 basic types of Galerkin integrals, depending on the domain of the outer (test) and inner integration, which may be a wire segment (L), a bilinear quadrilateral surface (S), or the volume of a trilinear hexahedron (V), and whether the integral kernel contains Green's function g given by (7) (potential integrals) or its gradient (field integrals). Thus, we have both potential and field Galerkin integrals of the type L/L, L/S, ..., S/V and V/V. They all contain power functions of parametric coordinates u, v, and w. For example, the potential integral corresponding to the test functions defined on the mth bilinear surface and the basis functions on the nth bilinear surface is given by

$$S_{mn} = \int_{-1}^{1} \int_{-1}^{1} u_m^i v_m^j$$
$$\cdot \left(\int_{-1}^{1} \int_{-1}^{1} u_n^k v_n^l g(R) \, du_n \, dv_n \right) du_m \, dv_m,$$
$$R = |\boldsymbol{r}_m(u_m, v_m) - \boldsymbol{r}_n(u_n, v_n)|. \tag{12}$$

Rapid and accurate integration methods are developed for the basic potential and field integrals (inner integration in the Galerkin integrals) of the L, S, or V type. Briefly, when the distance of the field point from the source point in g and ∇g is relatively small (or zero), the analytical procedure of extracting the (quasi-)singularity is performed. The procedure for evaluation of volume (quasi-)singular integrals in the case of analysis of dielectric scatterers is explained in detail in [12]. The procedure for evaluation of surface integrals consists of analytical integration of a principal (quasi-)singular part of the integrand over a (generally not rectangular) parallelogram whose surface is close to the surface of the bilinear quadrilateral near the singular point, and numerical integration of the rest using Gauss–Legendre quadrature formulas. The parallelogram that corresponds to the bilinear quadrilateral defined in (10) is defined by the following parametric equation:

$$\boldsymbol{r}'(u, v) = r_c' + \boldsymbol{r}_u' u + \boldsymbol{r}_v' v, \qquad -1 \leq u, v \leq 1;$$
$$\boldsymbol{r}_u' = \boldsymbol{r}_u + \boldsymbol{r}_{uv} v_0; \quad \boldsymbol{r}_v' = \boldsymbol{r}_v + \boldsymbol{r}_{uv} u_0;$$
$$\boldsymbol{r}_c' = \boldsymbol{r}(u_0, v_0) - \boldsymbol{r}_u' u_0 - \boldsymbol{r}_v' v_0 \tag{13}$$

u_0 and v_0 being the coordinates of the singular point at the surface. The extracted terms are proportional to $1/R^K$ and $[\boldsymbol{r}'(u, v) - \boldsymbol{r}_0]/R^K$, where $\boldsymbol{r}_0$ is the position vector of the projection of the field point onto the plane of the parallelogram, $K = 1$ for potential integrals, and $K = 3$ for field integrals. Analytical integration for $K = 1$ is done as proposed in [17], and an analogous procedure is developed for $K = 3$.

Finally, the algorithm for efficient nonredundant recursive construction of the Galerkin impedance matrix is utilized, in which, for any pair of geometrical elements, first and only once, the basic Galerkin integrals for all values of the power-functions indexes is recursively evaluated, and then simultaneously introduced into all impedances containing them. Note that, if the S/S integrals are considered and both bilinear surfaces are dielectric ones, there are 16 combinations for the corresponding impedances, relating to the u- and v-components of the vectors $\boldsymbol{J}_s$ and $\boldsymbol{M}_s$ over the two surfaces, and in all of them it is necessary to evaluate three different field terms. For example, the expression for the electric-field vector contains terms proportional to the magnetic vector potential, to the gradient of the electric scalar potential, and to the curl of the electric vector-potential [see (4)].

The resulting system of linear algebraic equations with complex current-distribution polynomial coefficients as unknowns is solved classically, by LU decomposition Gaussian elimination. Finally, the following quantities are obtained by post-processing of these coefficients:

- current distributions in individual geometrical elements;
- antenna admittance/impedance, reflection coefficient, voltage standing-wave ratio (VSWR);
- y-, z-, and s-parameters of EM multiport systems;
- electric and magnetic near field;
- losses in lumped and distributed resistive loadings;
- losses and specific absorption rate (SAR) distribution inside lossy dielectric bodies;
- overall losses and SAR, antenna radiation efficiency;
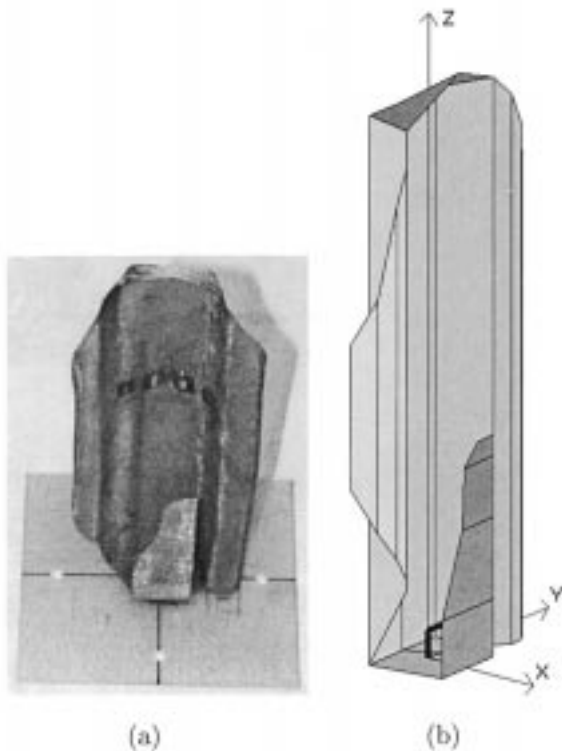- far field, antenna radiation patterns, and scatterer cross sections.

(a)   (b)

Fig. 4.   (a) Photograph and (b) simulated geometrical model of bat-ear antenna. The primary reflector is 165-mm high in the z-direction and 60-mm wide. The distance between the secondary reflector (*tragus*), which is 62-mm high and 21.5-mm wide in its base, and the back of the primary reflector is 23.5 mm (x-direction). The antenna feed is a folded wire monopole. The z- and y-directed wire segments are 7.5 –mm long each, and 0.7 mm in diameter. The distance of the monopole axis from the *tragus* is 12.5 mm.

Fig. 5.   Simulated and measured radiation pattern of antenna in Fig. 4 in plane $\phi = 0°$.

VI. PRACTICAL EXAMPLES

A. Bat-Ear Antenna

As the first example, consider a reflector antenna modeled after the external right-ear geometry of a bat species (*Plecotus auritus*), shown in Fig. 4(a). The measured dimensions of the ear [18] are normalized with respect to the acoustic wavelength at 50 kHz (navigation acoustic frequency of the bat), and the antenna (physical model) is fabricated from copper mesh with dimensions normalized to the EM wavelength at 10 GHz ($\lambda_0 = 3$ cm). The motivation is to benefit from the accuracy and sensitivity of bat biosonar systems in the design of direction-finding radar. The antenna consists of the primary (larger) and secondary (smaller) reflector, with a monopole feed, as described in Fig. 4.

This antenna is complex in shape and is about $5.5\lambda_0 \times 2\lambda_0 \times 1\lambda_0$ large. The simulated geometrical model, shown in Fig. 4(b), consists of 23 elements (two wire segments and 21 PEC bilinear surfaces). The number of unknowns for the approximation of currents in the MoM simulation amounts to 988. The CPU time required for the analysis, including post processing, is 8 min on a Pentium 166-MHz personal computer with 16-MB RAM memory.

Fig. 5 shows the simulated and measured radiation pattern of the bat-ear antenna in the plane $\phi = 0°$ (zenith plane) as a function of the angle θ. The pattern is measured in an anechoic
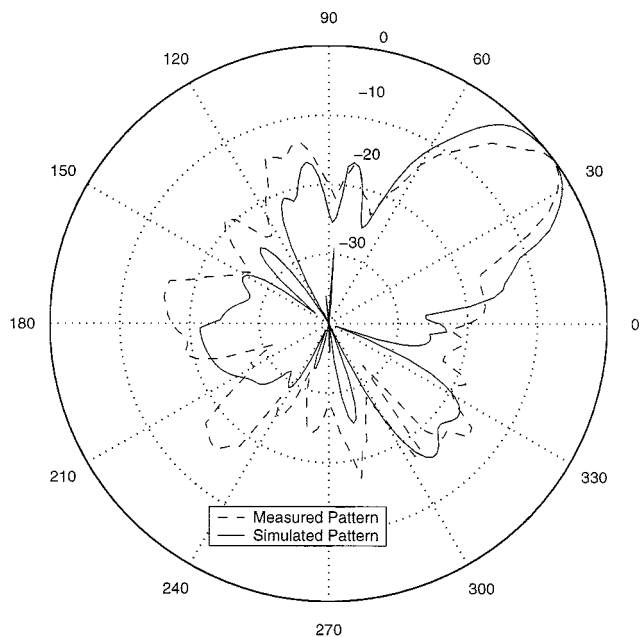
chamber with a fixed standard-gain horn antenna acting as a transmitter and the rotating bat-ear antenna as a receiver. The simulated and measured look (main-beam) directions $\theta_{\text{simulated}} = 37°$ and $\theta_{\text{measured}} = 36°$ are in excellent agreement, and also in good agreement with acoustic measurements at 50 kHz ($\theta_{\text{acoustic}} = 31.4° \pm 4°$) [18].

The convergence analysis was performed for this example. Three different levels of polynomial approximation of currents were adopted resulting in a total of 518, 988, and 1737 unknowns. The main-beam directions for the three solutions were $\theta_1 = 39°$, $\theta_2 = 37°$, and $\theta_3 = 37°$, respectively, and slight differences were noticed only in the low field region.

The small-domain version of the method, with rooftop basis functions, was also attempted. That was done by reducing the maximal extension of the computational subsurfaces in the code to $\lambda/10$ in each dimension. The discretization required the total of 11 160 unknowns to be determined, and the system matrix was far too large for the PC used. Note that the number of unknowns is for an order of magnitude larger when compared to the large-domain approach. Although this comparison is valid only for the particular small-domain solution, it is certainly at least indicative of numerical advantages of the large-domain (high-order expansion) MoM over the small-domain (low-order expansion) MoM.

B. Broad-Band Nested Planar Antenna Sub-Array

As the next example of application of the large-domain MoM code, consider a nested planar (horizontal) antenna sub-array, a top view of which is shown in Fig. 6. The motivation for this design is a multioctave reconfigurable array. Each element is a printed dipole antenna consisting of 14 PEC strips and 12 lumped line loads. (Note that our method/code includes models of point, line, and surface generators and loads, as well as arbitrary distributed loadings.) The dielectric is air. The large
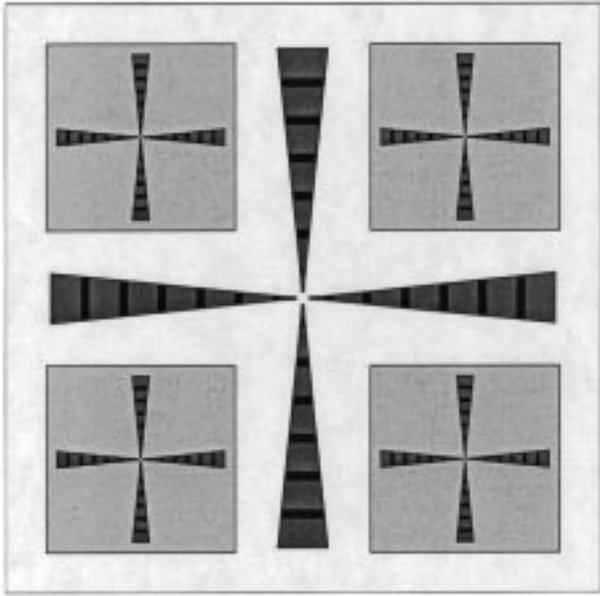
Fig. 6.   Top view of a nested planar horizontal loaded antenna sub-array with horizontal finite ground planes and vertical two-wire feed lines.

dipoles are 60-cm long, with the strip width increasing linearly from 1.2 mm at the feed to 12 mm at dipole free ends. The lumped loads are adopted to be approximately equivalent to the following continuously distributed resistive loading:

$$R_{\mathrm{p.u.l.}}(\omega, x) = \frac{\omega\mu_0}{4\pi}0.3e^{(\beta_0 x)^2} \ \Omega/\mathrm{m}, \qquad \beta_0 = \omega\sqrt{\epsilon_0\mu_0} \tag{14}$$

x being the distance from the dipole feed. These frequency- and position-dependent loads act as switches, which ensure the electrical length of the antenna be approximately constant in a broad frequency range. The computed return loss of the antenna (with respect to 600 Ω) is greater than 15 dB in a 3 : 1 frequency range (0.5–1.5 GHz). The antenna radiation efficiency is between 40%–72% in this range.

The basic broad-band elements are crossed for dual polarization, and scaled by a factor of three to cover the next frequency sub-band (1.5–4.5 GHz). Note that the scaling and nesting of dipoles can successively be continued for further 3 : 1 sub-bands. Each pair of crossed elements has a finite horizontal square ground plane that is a quarter-wavelength away at the central frequency of the sub-band. The element feeds are vertical two-wire transmission lines. Fig. 7 shows the simulation results for s_{11} and s_{33} of the sub-array, where ports 1 and 3 belong to one of the large and one of the small elements, respectively. The large ground is considered as infinite in the simulation, and taken into account by images. We observe that crossing of the elements of the same size and nesting of the elements of different sizes, as well as the addition of the ground planes and feed lines, have no significant effect on the broad-band circuit properties of the antenna elements in the corresponding frequency sub-bands. The simulation takes two minutes of CPU time at the highest frequency with a PC
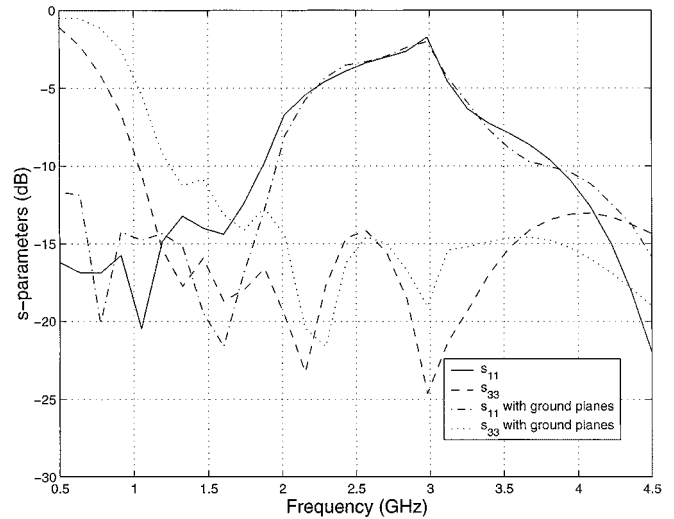

Fig. 7.   Simulated s_{11} (large dipoles) and s_{33} (small dipoles) of sub-array in Fig. 6, with and without ground planes, over the two operation sub-bands. The nominal impedances of all ports are 600 Ω.

Pentium 166 MHz. Note that the large elements are $9\lambda_0$ long at 4.5 GHz.

C. EM Coupling Between a Cellular-Phone Antenna and a Human Body

The volume-equivalence version of our large-domain method enables very efficient analysis of high permittivity/conductivity dielectric scatterers, such as biological tissues [10]. As an example, consider an EM system consisting of a person and an antenna of a cellular phone. The motivation is to analyze the influence of a person on the antenna properties. The antenna is approximated by an equivalent symmetrical center-fed wire dipole without the handset casing (Fig. 8). Let the frequency of the generator driving the antenna be $f = 840$ MHz, the dipole arm length $h = 8.45$ cm, and the radius of the wire $a = 0.127$ cm. The adopted model of a person is 178-cm high, and is made of a homogeneous lossy dielectric of parameters $\epsilon_r = 51.6$ and $\sigma = 1.56$ S/m, i.e., $\epsilon_{\mathrm{er}} = 51.6 - j33.38$ (taken from [3]). It is constructed with 12 trilinear hexahedrons, which are mostly of rectangular shape, as sketched in Fig. 8. As seen, the most attention is paid to modeling the shape of the human head, which has a dominant role in the EM coupling between the antenna and the body. Each antenna arm is represented as a single wire segment with polynomial approximation of current.

Table I shows the impedance of the dipole antenna for different distances d between the antenna and the face of the person ($x_g = 173.5$ cm). We can see that the dipole, which is almost resonant if situated in free space, is far from resonance if located close to the head. The antenna resistance is also greatly changed due to coupling with the human body. Our simulated results, which required 3 min of CPU time on a PC Pentium 166 MHz, are compared to the results obtained by the subdomain MoM using short wire segments and small dielectric cubes for geometrical modeling and pulse basis functions for the current/field approximation (the CPU time was 30 min with a CRAY-2 computer) [3]. Satisfactory agreement of the two sets of results can

TABLE I
IMPEDANCE OF A DIPOLE ANTENNA NEAR A MODEL MAN IN FIG. 8, FOR DIFFERENT DISTANCES d, OBTAINED BY OUR LARGE-DOMAIN METHOD (LDM) AND THE SUBDOMAIN METHOD [3]

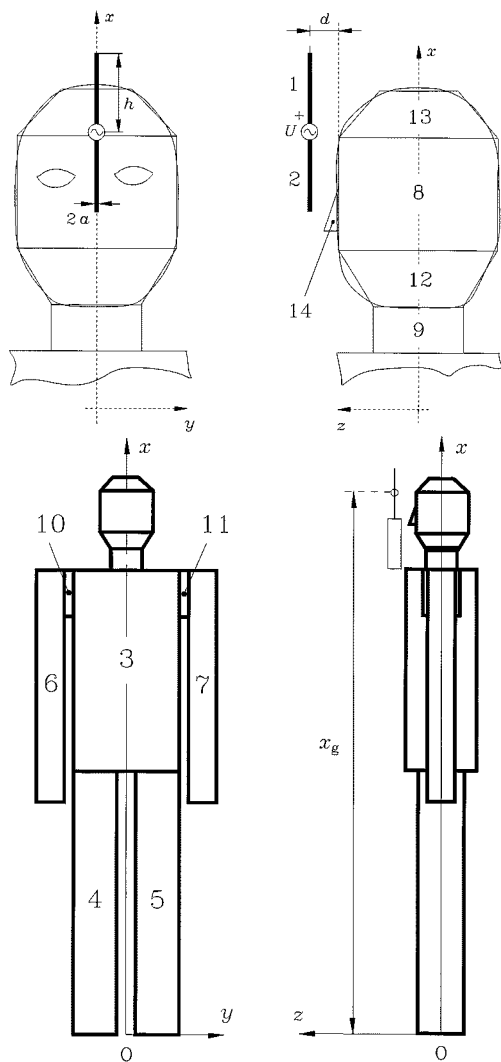|	$d \to \infty$	$d = 5$ cm	$d = 4$ cm	$d = 3$ cm	$d = 2$ cm	$d = 1$ cm
LDM	$(76.0 + \text{j}7.7)\,\Omega$	$(71.6 + \text{j}29.6)\,\Omega$	$(67.3 + \text{j}33.4)\,\Omega$	$(58.6 + \text{j}35.3)\,\Omega$	$(49.5 + \text{j}25.1)\,\Omega$	$(51.9 + \text{j}34.8)\,\Omega$
Ref.3	$(75 + \text{j}1.3)\,\Omega$	$(64 + \text{j}27)\,\Omega$	$(60 + \text{j}28)\,\Omega$	$(62 + \text{j}35)\,\Omega$	$(52 + \text{j}17)\,\Omega$	$(60 + \text{j}23)\,\Omega$

Fig. 8. Analysis of the EM coupling between a cellular-phone antenna and a human body—simulated geometrical model of the structure.
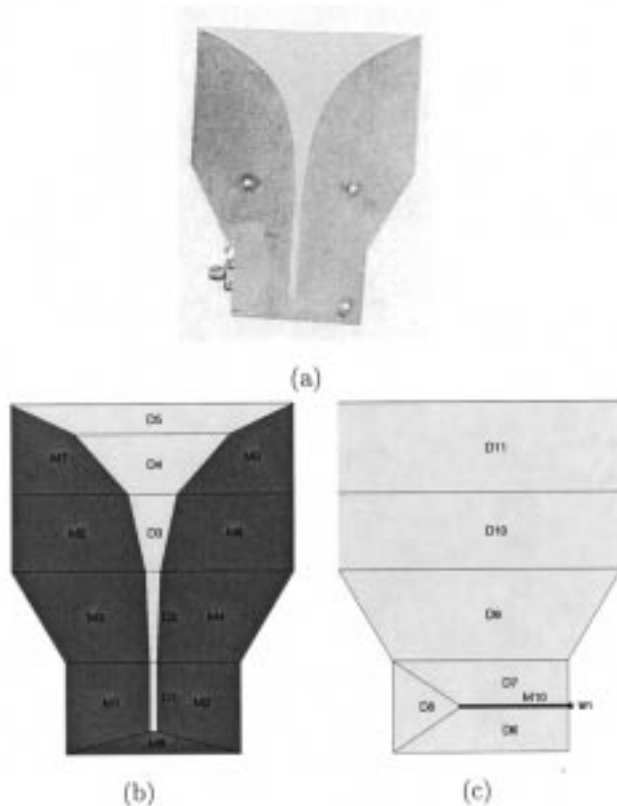

Fig. 9. (a) Photograph and (b)–(c) simulated geometrical model (front and back views) of microstrip-fed Vivaldi antenna. The thickness of the dielectric substrate is 1.27 mm, and the substrate relative permittivity 10.2. The length of the tapered slot is 108 mm, while its width varies from 2.4 to 93 mm. The length and width of the strip are 36 and 1.2 mm, respectively. The distance of the open-circuited end of the microstrip line from the slot axis is 7.2 mm, as is the distance of the slot line beginning from the strip axis.

D. Microstrip-Fed Vivaldi Antenna

As a final example, consider a microstrip-fed Vivaldi antenna, shown in Fig. 9(a). The motivation for this design is the need for an inexpensive scalable broad-band single element of a very large radio telescope based on a phased-array approach [19]. The antenna consists of a metalized dielectric substrate with an exponentially tapered slot in the metallization, and a crossed strip on the other side of the substrate. The strip and metallization form a microstrip line that feeds the slot antenna. The line

starts with a coaxial connector, and is left open at the end. The antenna was fabricated on a 50-mil-thick (1.27-mm) high dielectric-constant Duroid ($\epsilon_r = 10.2$) substrate. All the dimensions in the "feeding area" of the antenna are optimized by our MoM code, for a given dielectric substrate, to obtain maximal coupling between the microstrip and slot line in the operating frequency range. The code is utilized in the surface-equivalence version, which appears to be more suitable in cases when the metallic plates and the dielectric surfaces overlap exactly.

This structure is also quite complex and electrically large. Fig. 9(b) and (c) shows the simulated geometrical model of the antenna, which is constructed from 31 bilinear surfaces (ten metallic and 21 dielectric surfaces). The coaxial-line excitation is modeled by a short wire segment at the side of the substrate, with a lumped-point generator at its base. The computational surface is about $2.4\lambda_0^2$ (PEC–air interface) plus $24\lambda_d^2$
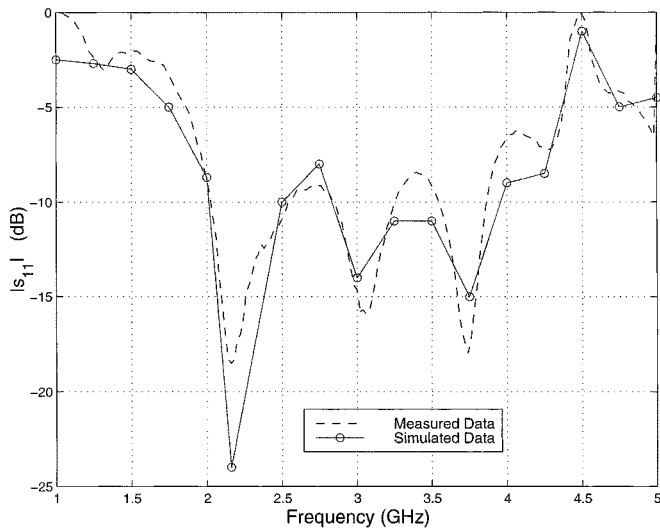
Fig. 10.   Simulated and measured reflection coefficient with respect to 50 Ω of antenna in Fig. 9.

(PEC–dielectric interface) plus $8.5\lambda_{\mathrm{mean}}^2$ (dielectric–air interface) large at the highest frequency (5 GHz). The corresponding total number of unknowns is 1024, and the CPU time 10 min on a PC Pentium 166 MHz.

Fig. 10 shows the simulated and measured reflection coefficient (with respect to 50 Ω) of the Vivaldi antenna in a frequency range of 1–5 GHz. The measurements were performed with an HP8510B network analyzer with a thru-reflect line (TRL) calibration. We observe excellent agreement between the two sets of results.

VII. CONCLUSIONS

This paper has presented a large-domain Galerkin-type MoM for the analysis of EM structures composed of arbitrarily excited and loaded dielectric and conducting bodies of arbitrary shapes. The method is based on the integral-equation formulation in the frequency domain. It is built and optimized in two versions concerning the type of the equivalence (volume and surface) invoked in the treatment of the dielectric parts of the structure and, consequently, the type of unknown quantities in the dielectrics. We have carefully chosen diverse and unconventional examples: the structures are electrically large (many wavelengths), they are complex in shape, some of them operate over a wide range of frequencies (several octaves), one example includes high permittivity/conductivity dielectrics, the dielectric layers are of finite extent, and the configurations are not rotationally symmetric. In all the examples, excellent modeling capabilities of bilinear quadrilaterals and trilinear hexahedrons in conjunction with polynomial current approximation have been demonstrated. The numerical data agree with experiment and other theoretical results, and the code has proven to be a useful and efficient design tool on a modest personal computer.

REFERENCES

[1] T. K. Sarkar, S. M. Rao, and A. R. Djordjevic, "Electromagnetic scattering and radiation from finite microstrip structures," *IEEE Trans. Microwave Theory Tech.*, vol. 38, pp. 1568–1575, Nov. 1990.

[2] A. P. M. Zwamborn and P. M. van den Berg, "The three-dimensional weak form of the conjugate gradient FFT method for solving scattering problems," *IEEE Trans. Microwave Theory Tech.*, vol. 40, pp. 1757–1766, Sept. 1992.

[3] H.-R. Chuang, "Human operator coupling effects on radiation characteristics of a portable communication dipole antenna," *IEEE Trans. Antennas Propagat.*, vol. 42, pp. 556–560, Apr. 1994.

[4] B. J. Rubin and S. Daijavad, "Radiation and scattering from structures involving finite-size dielectric regions," *IEEE Trans. Antennas Propagat.*, vol. 38, pp. 1863–1873, Nov. 1990.

[5] M. Gimersky and J. Bornemann, "A cellular-space-division-based method of moments algorithm for the pattern analysis of printed-circuit radiators," *IEEE Trans. Antennas Propagat.*, vol. 46, pp. 723–729, May 1998.

[6] S. M. Rao, C.-C. Cha, R. L. Cravey, and D. L. Wilkes, "Electromagnetic scattering from arbitrary shaped conducting bodies coated with lossy materials of arbitrary thickness," *IEEE Trans. Antennas Propagat.*, vol. 39, pp. 627–631, May 1991.

[7] M. Analoui and Y. Kagawa, "Electromagnetic scattering from conductor-coated material bodies," *Int. J. Numer. Modeling*, vol. 4, pp. 287–299, 1991.

[8] B. D. Popović, *CAD of Wire Antennas and Related Radiating Structures*.   New York: Wiley, 1991.

[9] B. M. Notaroš and B. D. Popović, "General entire-domain method for analysis of dielectric scatterers," *Proc. Inst. Elect. Eng.*, vol. 143, no. 6, pp. 498–504, 1996.

[10] ——, "Entire-domain analysis of high permittivity/conductivity 3D dielectric scatters," in *Journal of Applied Electromagnetism*.   Athens, Greece: Inst. Commun. Comput. Sci., 1997, vol. 1, pp. 1–12.

[11] ——, "General entire-domain Galerkin method for analysis of wire antennas in the presence of dielectric bodies," *Proc. Inst. Elect. Eng.*, vol. 145, no. 1, pp. 13–18, 1998.

[12] ——, "Optimized entire-domain moment-method analysis of 3D dielectric scatterers," *Int. J. Numer. Modeling*, vol. 10, pp. 177–192, 1997.

[13] B. M. Notaroš, "Numerical analysis of dielectric bodies of arbitrary shape and inhomogeneity in the electromagnetic field," Ph.D. dissertation, Dept. Elect. Eng., Univ. Belgrade, Belgrade, Yugoslavia, 1995.

[14] B. M. Notaroš, B. D. Popović, R. A. Brown, and Z. Popović, "Large-domain MOM solution of complex electromagnetic problems," in *IEEE MTT-S Int. Microwave Symp. Dig.*, Anaheim, CA, 1999, pp. 1665–1668.

[15] B. M. Notaroš, B. D. Popović, and Z. Popović , "EM simulations for radio and wireless on a PC," in *Proc. IEEE Radio Wireless Conf.*, Denver, CO, Aug. 1999, pp. 175–178.

[16] R. F. Harrington, *Field Computation by Moment Methods*.   New York: Macmillan, 1968.

[17] D. R. Wilton, S. M. Rao, A. W. Glisson, D. H. Schaubert, O. M. Al-Bundak, and C. M. Butler, "Potential integrals for uniform and linear source distributions on polygonal and polyhedral domains," *IEEE Trans. Antennas Propagat.*, vol. AP-32, pp. 276–281, Mar. 1984.

[18] R. B. Coles, A. Guppy, M. E. Anderson, and P. Schlegel, "Frequency sensitivity and directional hearing in the gleaning bat, Plecotus auritus (Linnaeus 1758)," *J. Comparative Physiol. A*, vol. 165, pp. 269–280, 1989.

[19] A. van Ardenne, "The SKA technical R & D program at NFRA," *NFRA Newslett.*, no. 15, pp. 1–7, Sept. 1998.

Branislav M. Notaroš (M'00) received the Dipl.Eng. (B.Sc.), M.Sc., and Ph.D. degrees in electrical engineering from the University of Belgrade, Belgrade, Yugoslavia, in 1988, 1992, and 1995, respectively.

From 1996 to 1999, he was an Assistant Professor at the University of Belgrade, where he taught electromagnetics and related courses. He is currently an Assistant Professor of electrical engineering at the University of Massachusetts, Dartmouth. He spent the 1998–1999 academic year as a Visiting Research Associate at the University of Colorado at Boulder.

He has authored or co-authored ten journal papers, 20 conference papers, six contract technical reports, three textbooks, and software. His research interests are in theoretical, computational, and applied electromagnetics.

Dr. Notaroš was the recipient of the 1999 Institution of Electrical Engineers (IEE) Marconi Premium.

Branko D. Popović (M'95) has been a Professor of electrical engineering at the University of Belgrade, Belgrade, Yugoslavia, for four decades. He was a Visiting Professor at the Virginia Polytechnical Institute, University of Colorado, McGill University, and Chengdu University. In 1999, he was with the wireless company Celletre Ltd., Haifa, Israel. He has authored or co-authored numerous papers on antennas and applied electromagnetics, six textbooks in fundamentals of electrical engineering and electromagnetics, three monographs on the analysis and computer-aided design (CAD) of wire and metallic antennas and scatterers, and two program packages.

Dr. Popović is a member of Serbian Academy of Sciences and Arts and is a Fellow of the Institution of Electrical Engineers (IEE), U.K. He was the recipient of the 1974 Institution of Electronics and Radio Engineers (IERE) Heinrich Hertz Premium, the 1985 IEE James Clerk Maxwell Premium, the 1985 Yugoslav Nikola Tesla Premium, the 1999 IEE Marconi Premium of the IEE, and numerous Yugoslav awards.

Jan Peeters Weem (S'99) received the B.S. degree in mathematics from Oregon State University, Corvallis, in 1994, the M.S. degree in applied mathematics from the University of Colorado, Boulder, in 1996, and is currently working toward the Ph.D. degree in applied electromagnetics (focusing on development of broad-band dual-polarization active antenna arrays for radioastronomy and phased arrays) at the University of Colorado, Boulder.

From 1996 to 1998, he was involved with numerical solutions to integral equations for EM problems at the University of Colorado.

Robert A. Brown, photograph and biography not available at time of publication.

Zoya Popović (S'86–M'90–SM'99) received the Dipl.Ing. degree from the University of Belgrade, Belgrade, Yugoslavia, in 1985, and the M.S. and Ph.D. degrees from the California Institute of Technology, Pasadena, in 1986 and 1990, respectively.

She is currently a Professor of Electrical and Computer Engineering at the University of Colorado, Boulder. She co-authored *Introductory Electromagnetics* (Englewood Cliffs, NJ; Prentice-Hall, 1999) and co-edited *Active and Quasi-Optical Arrays for Solid-state Power Combining*(New York: Wiley, 1997). Her research interests include microwave and millimeter-wave quasi-optical techniques and active antenna arrays, high-efficiency microwave circuits, RF photonics, and antennas and receivers for radioastronomy.

Dr. Popović was a recipient of the 1996 URSI International Issac Koga Gold Medal and was a 1993 NSF Presidential Faculty Fellow. She was the recipient of the 1993 IEEE Microwave Theory and Techniques Society (IEEE MTT-S) Microwave Prize for pioneering work in quasi-optical grid oscillators. She was named the Eta Kappa Nu Professor of the year by her University of Colorado students. In 2000, she was the recipient of a Humboldt Research Award from the German Alexander von Humboldt Stiftung.